Odor induces characteristic time courses of theta, beta and gamma oscillations in human olfactory cortex

Qiaohan Yang*[1], Guangyu Zhou[1], Gregory Lane[1], Christina Zelano[1]

[1]: Department of Neurology, Feinberg School of Medicine. Northwestern University. 320 E Superior Ave, Chicago IL. 60611

***, corresponding author**

Abstract

Neuronal oscillations are fundamental to cognition, facilitating coordination and communication of information within and across brain regions. Studies on the spectral and temporal dynamics of oscillatory rhythms have contributed substantial insight to our understanding of mechanisms of human visual, auditory and somatosensory perception. However, these oscillations have been largely unexplored in the human olfactory system, where we lack basic understanding of fundamental spectrotemporal and functional properties. Determining if and how dynamic signatures of neural activity occur in human olfactory cortex is critical to understanding how we process odors. Here, we establish a characteristic oscillatory response to an odor in the human brain. Using direct electrical recordings from human piriform cortex, we identified three key odor-induced rhythms, in the theta (4-8Hz), beta (13-30Hz) and gamma (30-150Hz) frequency bands, each with distinct functional and temporal properties. While theta emerges and dissipates rapidly at the start of inhalation, beta and gamma emerge later, with beta persisting through exhalation, and gamma peaking around the transition between inhalation and exhalation. Beta and gamma amplitudes strongly predict odor identification ability, whereas theta does not. Theta phase modulates beta and gamma amplitudes during inhalation, only when odor is present. Our findings establish that smells elicit distinct neuronal rhythms in human olfactory cortex, which are dynamically interplayed over the course of a sniff. Our data further suggest a fundamental role for beta and gamma oscillations in human olfactory processing, and that their amplitudes—organized by theta phase—subserve odor identification in humans.

Introduction

Local field potential oscillations are a fundamental feature of mammalian brain networks (Başar et al., 2001; Buzsáki, 2002; Engel & Fries, 2010; Fontanini & Bower, 2006; Fröhlich & McCormick, 2010; Heck et al., 2017; Kay et al., 2009; Lisman & Jensen, 2013; Zoefel & VanRullen, 2017). The earliest recordings of brain oscillations occurred in the olfactory system of hedgehogs (Adrian, 1942), leading to decades of highly productive research on oscillations in the mammalian olfactory system, mainly conducted in rodents (Beshel et al., 2007; Chapuis et al., 2013; Cohen et al., 2015; Courtiol et al., 2019; Fontanini & Bower, 2006; Frederick et al., 2016; Gnaedinger et al., 2019; Kay, 2005; Kay, 2014; Kay & Beshel, 2010; Kay et al., 2009; Kay & Stopfer, 2006; Lepousez & Lledo, 2013; Losacco et al., 2020; Lowry & Kay, 2007; Martin et al., 2007; Martin & Ravel, 2014; Mori et al., 2013; Neville & Haberly, 2003; Poo & Isaacson, 2009; Ravel et al., 2003; Rosero & Aylwin, 2011; Wilson & Sullivan, 2011; Zhou et al., 2017). However, 80 years later, we still lack a basic understanding of the role of these oscillations in olfactory processing in the human brain.

Work from rodents has identified oscillations in three key frequency bands that are associated with distinct olfactory processes: a slow theta rhythm (<8Hz), and two faster rhythms in beta (13-30Hz) and gamma (30-150Hz) bands (Beshel et al., 2007; Courtiol et al., 2019; Frederick et al., 2016; Kay, 2005; Kay & Beshel, 2010; Kay et al., 2009; Ketchum & Haberly, 1993; Lepousez & Lledo, 2013; Lowry & Kay, 2007; Martin & Ravel, 2014; Neville & Haberly, 2003; Ravel et al., 2003; Rosero & Aylwin, 2011; Zhou et al., 2017). Numerous studies have found strong associations between rodent theta oscillations and respiration (Fontanini & Bower, 2006; Jessberger et al., 2016; Kay, 2005; Kay & Stopfer, 2006; Macrides et al., 1982; Rojas-Líbano et

al., 2014; Verhagen et al., 2007), suggesting that theta oscillations in olfactory cortex track the respiratory cycle, potentially incorporating respiratory motor signals with odor processing (Kepecs et al., 2006; Schroeder et al., 2010). Rodent beta oscillations are linked to cognitive olfactory tasks, odor learning, and coherence between olfactory cortex and the rest of the brain (Frederick et al., 2016; Gnaedinger et al., 2019; Kay & Beshel, 2010; Martin et al., 2007; Martin & Ravel, 2014; Neville & Haberly, 2003), suggesting they likely play a role in long-distance communication related to olfactory processing (Martin et al., 2007; Martin & Ravel, 2014). Rodent gamma oscillations are linked to odor discrimination and identification tasks (Lepousez & Lledo, 2013; Losacco et al., 2020; Martin & Ravel, 2014), and increase with task difficulty (Beshel et al., 2007), suggesting they are important for fine odor perception, including distinguishing between similar odorants (Beshel et al., 2007; Lepousez & Lledo, 2013). Numerous rodent studies have found that the timing of odor-induced oscillations relative to sniff onset varies across frequency bands (Buonviso et al., 2003; Cenier et al., 2008; Courtiol et al., 2019; David et al., 2015; Litaudon et al., 2008; Lockmann et al., 2018; Manabe & Mori, 2013). While theta oscillations are linked to sniff onsets, beta oscillations increase during exhale (Buonviso et al., 2003; Cenier et al., 2008; Courtiol et al., 2019; Litaudon et al., 2008; Lockmann et al., 2018) and gamma oscillations increase at the peak of inhale, or around the transition between inhale and exhale (Manabe & Mori, 2013).

Against this background of wide-ranging rodent work, oscillations in human piriform cortex have been vastly understudied. We know little about the frequency and timing of odor-induced oscillations in human olfactory cortex. Relative to the abundance of rodent research, only a few studies have directly measured odor-induced oscillations in the human olfactory system (Hudry et al., 2001; Jiang et al., 2017; Jung et al., 2006). While odor-induced oscillations up to 40 Hz

have been recorded from the human amygdala (Jung et al., 2006), human piriform recordings suggest an important role for low frequency (< 8Hz) oscillations in olfactory processing (Jiang et al., 2017). Theta oscillations were consistently found in piriform cortex within 200ms of sniff onset during an odor detection task, whereas higher frequency oscillations were not (Jiang et al., 2017). Whether odors induce higher frequency oscillations in human piriform cortex, emerging at distinct phases of the sniff cycle, is unknown. Understanding if and how dynamic signatures of neural activity occur in human olfactory cortex is critical to understanding how we process odors.

In this study, we used stereotactic intracranial electroencephalography (iEEG) to test three main hypotheses about odor-induced local field potential oscillations in human piriform cortex during an olfactory identification task. First, that odors would induce theta, beta and gamma oscillations in human piriform cortex. Second, that the timing of odor-induced responses would vary across the different frequency bands. Third, that features of odor-induced beta and gamma oscillations would better predict task performance compared to theta oscillations.

Results

To examine odor-induced oscillations in human olfactory cortex, we recorded local field potentials from 7 participants who took part in an odor identification task. Each participant's clinical electrode coverage included a contact in piriform cortex (**Fig. 1A**). The olfactory task was performed during clinical recording of ongoing electrophysiological activity, at sampling rates ranging between 500 to 2000Hz, using a 256-channel clinical EEG acquisition system

(Nihon Kohden). Each trial began with an auditory cue signaling that odor would be presented, and providing the potential identity of the odor (rose or mint). After a jittered delay (3 to 7 s), odor was presented to the participant while sniff onset was precisely measured via a pressure sensor at the nose (Salter Labs). On each trial, participants identified the odor by indicating whether or not it matched the identity prompt (**Fig. 1B**). To isolate effects induced by odor from those induced by inhalation, which also impacts oscillations in human piriform cortex (Herrero et al., 2018; Mainland & Sobel, 2006; Sobel et al., 1998; Zelano et al., 2016), we analyzed and directly compared LFPs during inhalations that contained odor and those that did not, resulting in two experimental conditions: odor and no-odor (**Fig. 1B**, areas shaded in pink and blue).

Figure 1

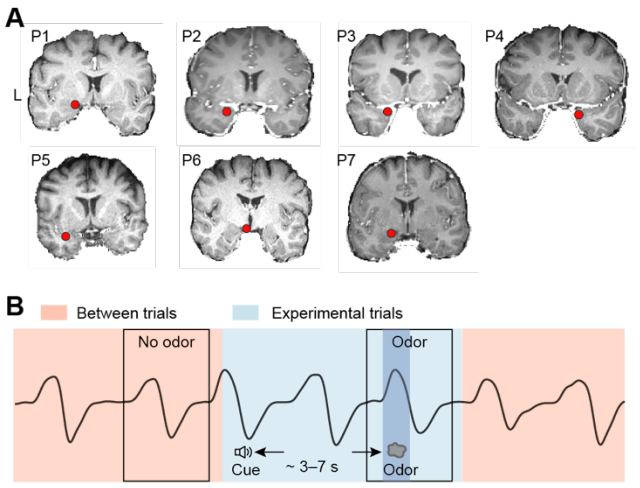

Odor induces oscillations in theta, beta and gamma frequency bands in human piriform cortex

To test the hypothesis that odor induces LFP oscillations in the theta, beta and gamma frequency bands in human piriform cortex, we first conducted a time-frequency analysis combining data from all trials and participants. We computed spectrograms aligned to sniff onset, for odor and no-odor conditions separately. In the odor condition, we found statistically significant increases in theta, beta and gamma frequency bands (**Fig. 2A,** left panel) (theta peak: 4.72 Hz, max z score = 14.07; beta peak: 18.98 Hz, max z score = 8.11; gamma peak: 84.94 Hz, max z score = 4.88). In the no-odor condition, we found smaller but significant increases in theta only (**Fig. 2A**, middle panel, peak: 4.02 Hz, max z score = 3.44). To quantify the difference between odor and no-odor conditions, we conducted a direct statistical comparison by permuting condition labels to generate a map of z-normalized amplitude differences (**Fig. 2A**, right panel). We found that theta, beta and gamma amplitudes were significantly higher in the odor compared to the no-odor condition ($p < 0.05$, FDR corrected, permutation test).

To confirm our findings at the individual level, we next computed sniff-aligned spectrograms in each participant separately (**Fig. 2B-C**). We found consistent increases in theta, beta and gamma amplitude in each individual participant in the odor condition, but not in the no-odor condition (**Fig. 2B-C**, black outlines indicate statistical significance via permutation test FDR corrected for multiple comparisons, $p < 0.05$). We then computed a direct statistical comparison between the two conditions for each participant (**Fig. 2D**). We found that amplitudes in all three frequency bands were significantly stronger during the odor compared to the no odor condition (paired sample t test, theta: $t(6) = 3.19$, $p = 0.0187$; beta: $t(6) = 4.17$, $p = 0.0059$; gamma: $t(6) = 2.98$, $p = 0.0245$). Notably, in every single participant, theta, beta and gamma amplitudes were larger during the odor compared to the no-odor condition. Together, these results suggest that odor consistently induces distinct theta, beta and gamma oscillations in human piriform cortex.

Figure 2

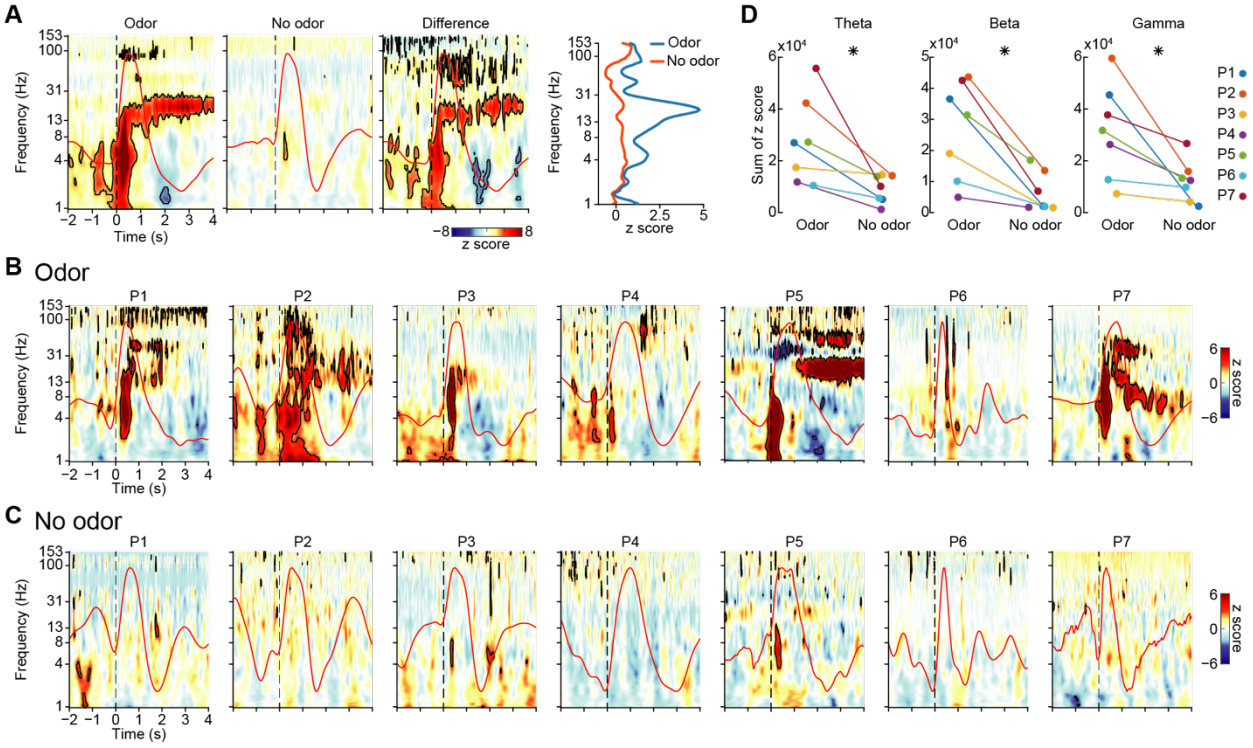

The time course of odor-induced oscillations varies across frequency bands

The spectrograms in figure 2 showed apparent variable time courses of odor-induced oscillations relative to sniff onset across frequency bands (**Figs. 2A-B**). Theta appeared to emerge and dissipate soonest, with beta and gamma emerging later and persisting longer. To quantify these differences, we conducted a series of analyses to characterize the timing of responses across frequency bands. These included a percent-change analysis to examine oscillatory increases over time, a bootstrapping analysis to minimize potential impact of noisy trials, a cluster-based analysis to quantify the exact timing and magnitude of continuously significant increases in oscillatory amplitude, and a circular-distribution analysis to examine oscillatory peaks over respiratory phase.

In our first analysis, we calculated the percent change in amplitude for each frequency band at each time point, for each condition (**Fig. 3A**). This allowed us to determine the timing of the emergence of significant differences between odor and no-odor conditions (FDR corrected $p < 0.05$, paired t test). This analysis showed distinct temporal dynamics of odor responses for each frequency (**Fig. 3A**, black lines above each panel). Odor-induced theta oscillations were the earliest to emerge and dissipate, beginning 126ms prior to sniff onset and ending 516ms after sniff onset. Gamma oscillations emerged next, 116ms after sniff onset, intermittently persisted through exhalation, and dissipated 3,678ms after sniff onset. Beta oscillations emerged last, 144ms after sniff onset, and persisted longest, ending 3,786 ms after sniff onset.

In a second analysis, designed to minimize the contribution of noisy trials and statistically evaluate the time courses, we tested whether differences in temporal dynamics of odor-induced responses across frequency bands were stable across resampled sets of trials. We conducted a bootstrapping analysis to create separate profiles of the timing of odor-induced responses for each frequency band. We created a z-normalized time series of resampled mean values for each frequency band, represented as a colormap (**Fig. 3B**, y-axis is each bootstrap repetition). We found stable time courses across repetitions, indicated by stripes of increased amplitude at particular times for each frequency band. To quantify the timing of amplitude increases, we performed a cluster-based statistical analysis; for each frequency band, we generated a t-statistic at each time point for all z-normalized odor trials, and then conducted a permutation-based analysis to correct for cluster size. We found clusters that corresponded well with the spectrograms shown in figure 2, with the percent-change analysis, and with the bootstrap analysis (**Fig. 3C**). We found one significant cluster for the theta band extending 266ms pre sniff to 810ms post sniff ($p < 0.0001$, permutation test), one for the beta band extending from 238ms

to 3524ms post sniff ($p < 0.0001$), and four separate clusters for the gamma band (326ms to 452ms post sniff, $p = 0.0346$; 764ms to 892ms post sniff, $p = 0.0145$; 1374ms to 1642ms post sniff, $p < 0.0001$; 1902ms to 2016ms post sniff, $p = 0.0451$). We subsequently conducted the same bootstrapping analysis at the single subject level, and plotted the average time point of each subject's bootstrapped peak distribution on top of the significant clusters in figure 3C (see overlayed dots, each representing the peak value for a single participant, with lines connecting individual values across frequencies). Although single participant data was more variable, beta and gamma peaks occurred later than theta peaks for almost all subjects. These results suggest that the unique time courses of odor responses across frequencies were unlikely to be caused by noise, spikes, and other artifacts.

In a third analysis, designed to account for individual respiratory differences in the time domain, we examined the circular distributions of oscillatory peaks over the respiratory phase. On each repetition of a bootstrapping analysis, the peak amplitude and corresponding phase angle were calculated from the average LFP and respiratory time series. We found that theta peaks narrowly aggregated at early stages of inhale (mean phase angle = -0.67 rad, PLV = 0.99, Rayleigh's $z = 998.05$, $p < 0.0001$) (**Fig. 3D**, left), consistent with previous findings in humans (Jiang et al., 2017). By contrast, beta peaks consistently aggregated at the exhale trough (mean phase angle = 2.98 rad, PLV = 0.80, Rayleigh's $z = 647.78$, $p < 0.0001$) (**Fig. 3D**, middle). Gamma peaks were more broadly distributed, with most centered around inhale peak or the transition between inhale and exhale (mean phase angle = 0.57 rad, PLV = 0.63, Rayleigh's $z = 401.69$, $p < 0.0001$) (**Fig. 3D**, right). Combined, these findings suggest that odor-induced theta oscillations increase earlier than beta and gamma oscillations, and that while theta and gamma oscillations are maximal during inhalation, beta oscillations peak during exhale.

Figure 3

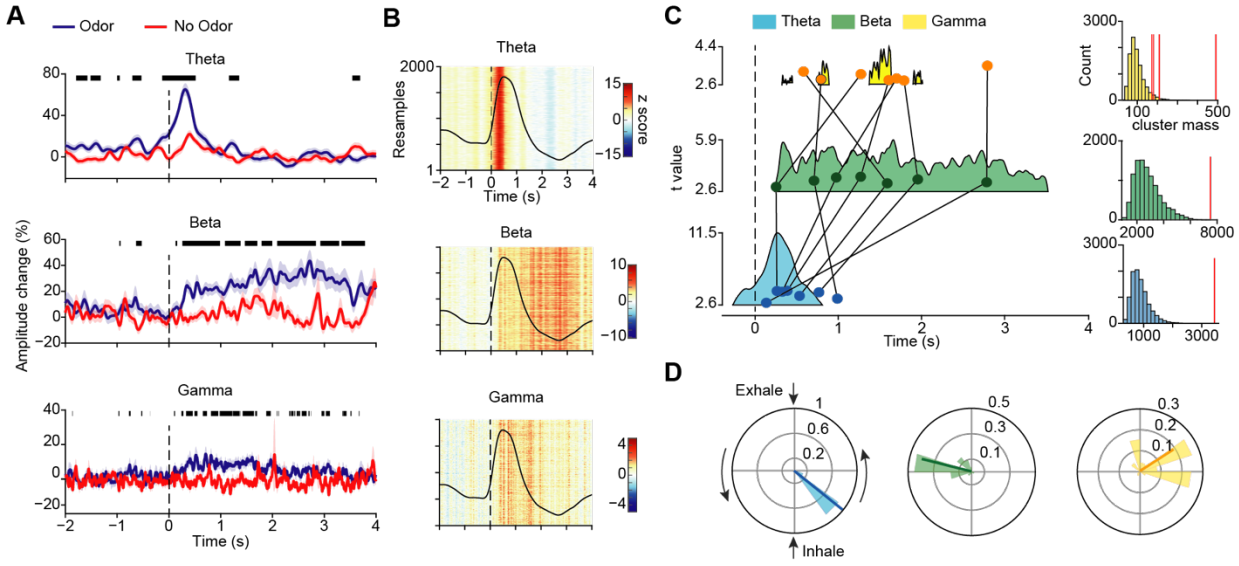

Beta and gamma oscillations outperform theta at predicting odor identification accuracy.

Numerous rodent studies suggest that beta and gamma oscillations relate to odor learning and discrimination, through both local odor coding (Beshel et al., 2007; Frederick et al., 2016; Losacco et al., 2020; Martin & Ravel, 2014; Ravel et al., 2003) and recruitment of larger-scale networks (Frederick et al., 2016; Gnaedinger et al., 2019; Kay & Beshel, 2010; Martin et al., 2007; Martin & Ravel, 2014; Mori et al., 2013). We therefore hypothesized that beta and gamma oscillations in human piriform cortex would correlate more strongly with task performance than theta. We conducted three separate analyses to explore the relationship between odor-induced LFP oscillations and odor identification accuracy. These included a combined time-frequency analysis to look for gross differences between correct and incorrect trials, a correlation analysis to look for a relationship between accuracy and oscillations across trials, and a machine learning analysis to determine whether amplitudes of different frequency responses could predict accuracy.

First, in a combined time-frequency analysis, we computed spectrograms of odor-induced responses during correct and incorrect trials separately, in order to look for differences across frequency bands. We found that during trials in which the participant correctly identified the odor, there were statistically significant increases in theta, beta and gamma band amplitudes (**Fig. 4A**, left panel, FDR corrected $p < 0.05$). By contrast, during trials in which the participant failed to identify the odor, statistically significant increases were found only in the theta band, with no such increases in the beta or gamma bands (**Fig.4A, right panel,** FDR corrected $p < 0.05$). Since most participants performed above chance on the task, there were a larger number of correct trials than incorrect trials (252 versus 71). To account for this difference and to directly statistically compare spectrograms for correct and incorrect trials, we conducted a resampling analysis in which correct and incorrect trials were resampled with replacement to include the same number of trials on each repetition, and we computed the distribution of the difference values (correct – incorrect) across each frequency band. We found statistically significantly larger responses during correct compared to incorrect trials for beta and gamma bands only, with no significant differences in the theta band. (one sample t test against 0 for the difference distribution. theta: $t(199) = 1.21$, $p = 0.2247$; beta: $t(199) = 35.55$, $p < 0.0001$; gamma: $t(199) = 42.61$, $p < 0.0001$. Paired sample t test for difference in theta and beta bands: $t(199) = -41.02$, $p < 0.0001$; Paired sample t test for beta and gamma: $t(199) = 17.36$, $p < 0.0001$; Paired sample t test for gamma and theta: $t(199) = 37.10$, $p < 0.0001$.). Notably, there were not sufficient numbers of incorrect trials for every participant to conduct this analysis at the individual level.

Second, we looked for a relationship between task performance and odor-induced responses in each frequency band on a trial-by-trial basis. To account for differences in frequency bands over time, we conducted this analysis during the inhale and exhale periods separately. Trials were

subsampled to generate a distribution of correlation coefficients representing the relationship between oscillatory amplitude and accuracy for each frequency band. Significant correlations between accuracy and amplitude were evident in the beta and gamma bands during both inhale and exhale (one tailed one sample t test against FDR corrected threshold for significant correlation coefficient; beta during inhale: $t(49) = 31.25$, $p < 0.0001$; beta during exhale: $t(49) = 17.64$, $p < 0.0001$; gamma during inhale: $t(49) = 23.70$, $p < 0.0001$; gamma during exhale: $t(49) = 28.25$, $p < 0.0001$.), but no such correlation was found in the theta band (theta during inhale: $t(49) = -2.04$, $p = 0.97$; theta during exhale: $t(49) = -12.90$, $p = 1$). In line with this, a direct statistical comparison across frequency bands showed that correlations were significantly stronger between task accuracy and amplitude for beta and gamma bands compared to theta band during both inhale and exhale time periods (**Fig. 4C**). **(**two way repeated measure ANOVA: main effect of time window: $F(1, 49) = 111.08$, $p < 0.0001$; main effect of frequency band: $F(2,98) = 547.98$, $p<0.0001$. paired sample t test across frequency bands during inhale for theta and beta: $t(49) = -29.37$, $p < 0.0001$; for beta and gamma: $t(49) = 3.11$, $p = 0.0031$; for gamma and theta: $t(49) = 24.95$, $p < 0.0001$; paired sample t test across frequency bands during exhale for theta and beta: $t(49) = -26.51$, $p < 0.0001$; for beta and gamma: $t(49) = -11.13$, $p < 0.0001$; for gamma and theta: $t(49) = 33.95$, $p <0.0001$).

Finally, we used machine learning to perform a classification analysis on inhale and exhale amplitudes for each frequency band, to determine whether these features could predict task accuracy. To this end, we applied a binary linear support vector machine (SVM) classifier to the data, plotted the receiver operative characteristic (ROC) curves and calculated the area under curve (AUC), which was used together with optimized classifier accuracy as the predictor of data separability. We found that beta and gamma amplitudes were highly successful at separating the

trials by accuracy, while theta amplitudes were less so (**Fig. 4D**). Specifically, gamma accuracy was maximal at 91.5%, beta accuracy was also high at 91%, whereas theta accuracy was lower, at 66.5%. This same procedure was applied to shuffled data, which resulted in chance performance (accuracy = 52%), validating our methods. These findings correspond well with the results from the two previous analyses, and, taken together, suggest that beta and gamma band amplitudes are more strongly correlated with task performance than theta amplitudes.

Figure 4

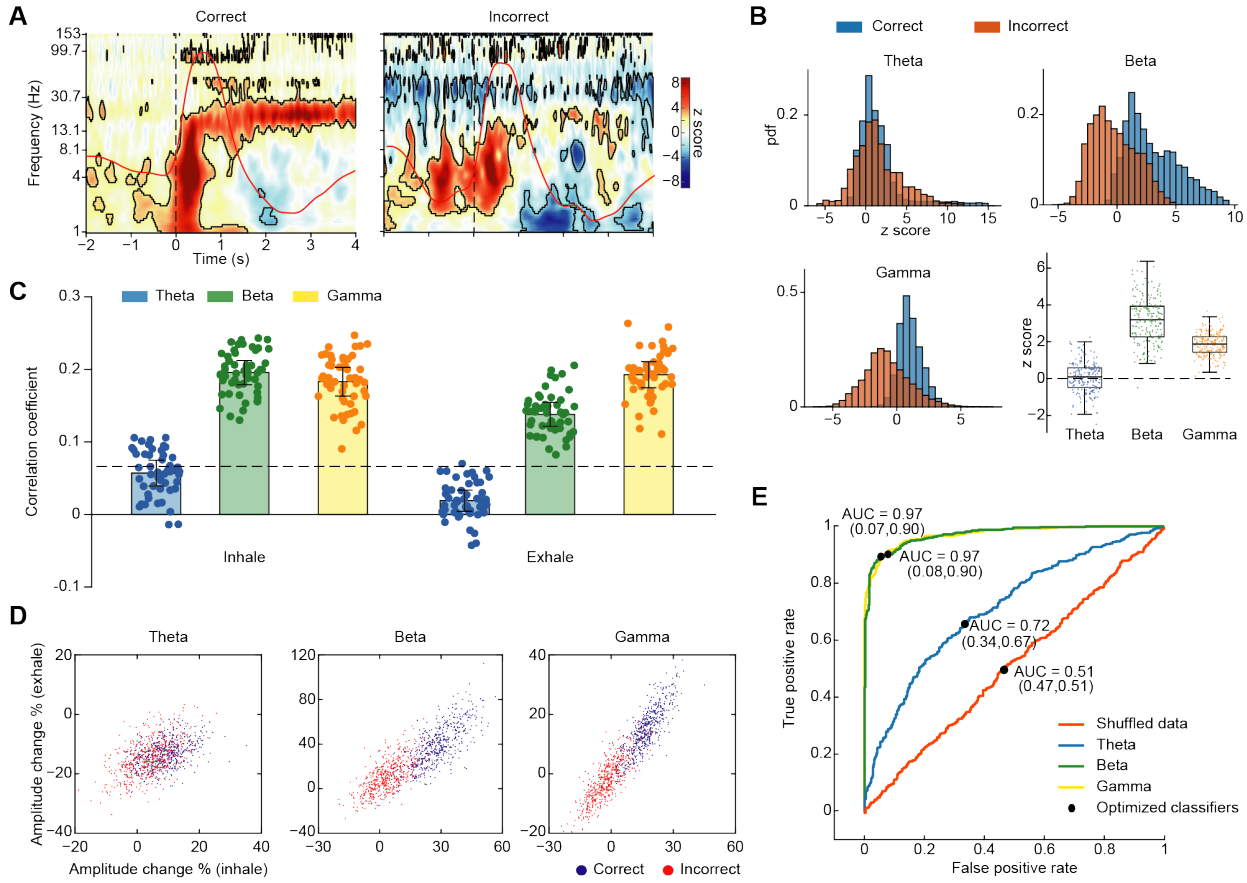

Odor-induced high-frequency oscillations were not driven by attention.

Because the odor condition occurred during experimental trials and the no-odor condition occurred between experimental trials, responses during the odor condition could potentially have been impacted by attentional states that were not present during the no-odor condition. Previous human and rodent work suggests that olfactory cortical responses are modulated by attention (Carlson et al., 2018; Zelano et al., 2005), particularly in lower frequency LFPs (Arabkheradmand et al., 2020; Zhou et al., 2019). To control for potential effects of attention on our findings, we analyzed odorless sniffs taken in attended states during experimental trials. Each trial began with a cue, followed by a delay (3 to 7s) prior to presentation of odor. Therefore, during many trials, sniffs of clean air occurred between the cue and odor (**Fig. 5A**). These sniffs occurred during attended states, but did not contain odor, thus providing a means to isolate the effects of attention from the effects of odor. Because a sniff did not always occur between the cue and the odor, the number of trials in the attended odorless condition was lower than the odor condition. Therefore, we subsampled odor trials to match the number across conditions. We computed spectrograms aligned to attended odorless sniffs and compared them to those aligned to odor sniffs (**Fig. 5B**, left and middle). We found that attended odorless sniffs induced oscillations in low frequencies (below 8 Hz) only ($p < 0.05$, FDR corrected), and found no stable higher frequency oscillations (> 8Hz). We then computed the z-normalized difference across conditions (**Fig. 5B**, right) and found significant differences between attended odor trials and attended no-odor trials in the theta, beta and gamma bands, such that oscillations in all three frequency bands were increased when odor was present, even after removing the effects of attention (**Fig. 5B**, right, $p < 0.05$, FDR corrected). Since theta oscillations were still detected in the attended no-odor condition, these findings suggest that the odor-induced increases in beta and

gamma bands were independent of attention, whereas theta band increases reflected, at least to some degree, attentional states.

Figure 5

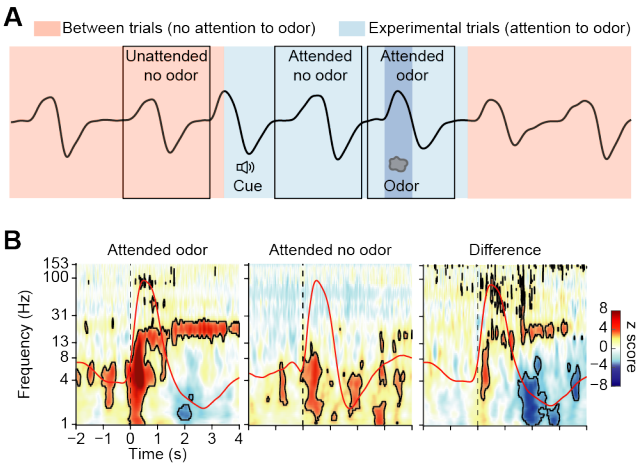

Theta phase modulates high frequency oscillatory amplitude during inhale.

Previous work suggests that odor-induced theta oscillations predict odor identities, even during a detection task that does not require participants to identify odors (Jiang et al., 2017). Here, we found that odor-induced theta oscillations were less correlated with odor identification performance than beta and gamma oscillations. However, theta rhythms in our data were evidently driving beta responses, which appeared to oscillate at around 5 Hz during inhale (**Fig. 5A**, see grey box). We hypothesized that theta oscillations might organize later-emerging higher frequency oscillations through phase modulation. To estimate modulation of higher frequency amplitude by theta phase, we calculated the modulation index (MI) (Tort et al., 2010) using theta phase as the modulating signal and a range of high frequencies (13 – 150 Hz) as the amplitude signals, for both odor and no-odor conditions (**Fig. 5B**). We found that in the 1s time window following sniff onset, theta phase significantly modulated beta and gamma oscillations (FDR corrected $p < 0.05$) during the odor condition (FDR corrected $p < 0.05$ for MI in all frequency

bands, peak MI at 16.16 Hz, max z score = 17.67, z score = 7.52+-3.69) , but not during the no odor condition (z score = 2.02+-1.57). This finding suggests that higher frequency oscillations were modulated by theta phase during the early period of sniffing, when theta amplitudes were significantly increased.

Figure 6

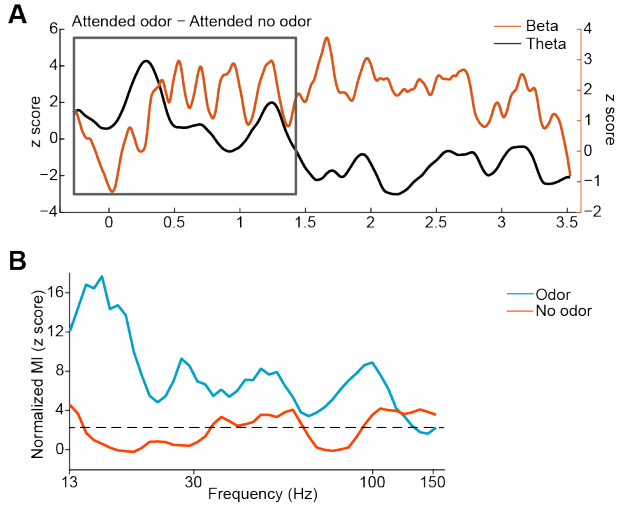

Discussion

We found odor-induced oscillations in human piriform cortex in the theta, beta and gamma frequency bands, each with distinct temporal dynamics, forming the basis of a characteristic human olfactory cortical response. While theta oscillations rapidly emerged, peaked and dissipated within the first 500ms of inhalation, gamma and beta oscillations emerged and peaked later, extending into the exhale period. These findings suggest that the spectrotemporal characteristics of odor-induced oscillations in piriform cortex are similar in rodents and humans. We further found that the strength of beta and gamma oscillations was significantly more

correlated with odor identification accuracy than theta oscillations, suggesting beta and gamma rhythms are important for odor identification in humans.

Interestingly, we found that gamma rhythms were more tightly correlated to odor identification accuracy than beta during exhale. Since gamma rhythms are thought to reflect local computations (Beshel et al., 2007; Buzsáki & Wang, 2012; Frederick et al., 2016; Kopell et al., 2000; Lepousez & Lledo, 2013; Losacco et al., 2020; Martin & Ravel, 2014; Ravel et al., 2003), and beta oscillations are thought to reflect long-range network interactions (Frederick et al., 2016; Gnaedinger et al., 2019; Kay & Beshel, 2010; Kopell et al., 2000; Martin et al., 2007; Martin & Ravel, 2014), local computations in piriform cortex may have particular significance during exhale. Our data also highlight an important role for theta oscillations in human piriform cortex, in agreement with previous studies (Jiang et al., 2017), as we found that theta phase modulated beta and gamma amplitudes during inhalation, only when odor was present. Thus the theta rhythm may participate in the organization of sensory information processing in human piriform cortex.

Theta, beta and gamma oscillations have been extensively studied in the olfactory systems of rodents, providing insights into the functional roles of these oscillations in olfactory perception (Beshel et al., 2007; Chapuis et al., 2013; Courtiol et al., 2019; Frederick et al., 2016; Fukunaga et al., 2014; Gnaedinger et al., 2019; Kay, 2005; Kay, 2014; Kay & Beshel, 2010; Kay et al., 2009; Kay & Stopfer, 2006; Ketchum & Haberly, 1993; Losacco et al., 2020; Lowry & Kay, 2007; Martin et al., 2007; Martin & Ravel, 2014; Mori et al., 2013; Neville & Haberly, 2003; Poo & Isaacson, 2009; Rosero & Aylwin, 2011; Stopfer et al., 1997; Zhou et al., 2017). Furthermore, an impactful body of rodent work has shown that the timing of olfactory responses

relative to sniffing behavior is an important mechanistic feature of odor coding, enabling accurate olfactory percepts to form quickly (Bathellier et al., 2008; Blauvelt et al., 2013; Grosmaitre et al., 2007; Kepecs et al., 2006; Losacco et al., 2020; Phillips et al., 2012; Rennaker et al., 2007; Rosero & Aylwin, 2011; Shusterman et al., 2011; Uchida et al., 2006; Verhagen et al., 2007). Though much of this work has focused on the olfactory bulb, responses in rodent piriform cortex also include temporal modulations (Bolding & Franks, 2017; Haddad et al., 2013; Rennaker et al., 2007), and its oscillations reflect sniff phase (Courtiol et al., 2019; Herrero et al., 2018; Litaudon et al., 2008). In contrast to the extensive and elegant body of rodent work, oscillations in human piriform cortex have been vastly understudied. Here, dovetailing with rodent work, we found that theta, beta and gamma oscillations emerged at different times relative to sniff onset. The link between sniffing behavior and oscillations in rodents, combined with dramatic differences in sniffing behavior between rodents and humans, raises some intriguing questions about the timing of odor responses in humans. When sampling odors, rodents engage in multiple sniffing strategies, and may sniff at rates up to 12Hz (Frederick et al., 2017; Kepecs et al., 2007; Sirotin et al., 2014; Wesson et al., 2008). Humans might increase their sniffing frequency a bit when smelling something, but often sample odors in a single sniff, and aren't able to reach sniffing frequencies of 12Hz (though this has not been directly tested yet). Despite these large differences in sniffing behaviors across species, we found surprisingly similar time courses of odor responses in piriform cortex. For example, Frederick et. al. (2016) found that odor-evoked beta oscillations in rodent piriform cortex emerged at around 200ms following odor onset, similar to our findings in human piriform cortex. We found that beta oscillations peaked and persisted longer than gamma oscillations, also in agreement with findings in rodents (David et al., 2015). In rodents, the theta rhythm is actively shaped by sniffing behavior, which, in turn,

shapes higher frequency oscillations. In humans, sniffing behavior almost never occurs at frequencies near the theta range, yet interestingly, we found that theta oscillations shape higher frequency oscillations in the human olfactory system during inhalation, as is the case in rodents. This may suggest that the time scale of some odor-induced oscillations is not entirely dependent on breathing rate, and that network properties that support these rhythms are likely conserved across species. Our findings support the idea that the theta rhythm serves as the "internal reference clock" of odor information processing (Jiang et al., 2017), though future studies combining data from both humans and rodents, and potentially from noninvasive human olfactory bulb recordings (Iravani et al., 2020) could contribute much needed insights to answer this question.

We found that the magnitude of beta and gamma oscillations predicted odor identification accuracy, whereas theta did not, offering support for distinct functional roles for the different rhythms in olfactory processing (Beshel et al., 2007; Frederick et al., 2016; Kay & Beshel, 2010; Martin & Ravel, 2014). Establishing beta rhythms in human piriform cortex may also lay the groundwork for future work on olfactory networks and integration of olfactory information with other cognitive processing streams and behaviors (Kay & Beshel, 2010). For example, integration of olfactory information with language networks (Majid, 2020; Majid & Kruspe, 2018; Olofsson & Gottfried, 2015), memory networks (Arshamian et al., 2018; Arzi et al., 2014; Wilson & Stevenson, 2003; Yeshurun et al., 2009), sleep states (Arzi et al., 2010; Hauner et al., 2013; Perl et al., 2016; Rasch et al., 2007), and other olfactory-guided behaviors (Bhutani et al., 2019; Howard et al., 2020) could potentially involve interactions in beta oscillatory networks. Though our data suggest particular importance for beta and gamma oscillations in odor perception, we also found that the phase of theta oscillations modulated beta and gamma

amplitudes during inhalation. Interestingly, we found that theta oscillations, but not beta or gamma oscillations, increased during attended states when no odor was present (**Fig. 5B**), and even prior to sniffing when odor was expected (**Fig. 2A; Fig. 3A; Fig. 3C**). Taken together, these findings may indicate a role for theta in olfactory attention, in line with numerous previous studies suggesting that lower frequency oscillatory phases and amplitudes reflect attentional states in the human brain (Arabkheradmand et al., 2020; Kam et al., 2019; Zhou et al., 2019). Olfactory attention also shapes neural responses in rodent olfactory cortex (Carlson et al., 2018), and potential future work may include a direct comparison of these oscillations between species. It may also be interesting to explore these oscillations in other primary olfactory areas which may have similar neural responses as piriform cortex (Iurilli & Datta, 2017; Millman & Murthy, 2020; Moberly et al., 2018).

Overall, our findings begin to define a characteristic human spectrotemporal odor response, consisting of three distinct frequency bands with unique time courses relative to sniff onset, and corresponding closely with cortical responses that have been found in rodents. This lays the groundwork for future work to further explore the functional role of the different aspects of the human cortical olfactory response.

Figure Legends

Figure 1: Electrode contact locations and experimental design. **A**. The location of the piriform cortex electrode contact (red dot) is shown on each participant's brain image. L, left hemisphere. **B**. Schematic illustration of the olfactory task, showing odor and no-odor conditions drawn on an illustrative breathing signal (black line). The light blue area indicates experimental trials (starting

from cue delivery to the end of the breathing cycle in which odor was delivered), and the pink area indicates between trials. The black boxes indicate the analysis time windows for odor and no-odor trials. The darker blue area indicates odor delivery.

Figure 2: Odor induces theta, beta and gamma oscillations in human piriform cortex. **A**. Results from combined analysis showing z-normalized amplitude spectrograms for odor and no-odor conditions (left and middle panels), and the difference between the two (right panel). Average respiratory signal is shown on each panel (overlaid red line). Dashed line represents inhale onset. For odor and no-odor spectrograms, the black contour lines indicate statistical significance of permutation tests against pre-cue baseline, after FDR correction for multiple comparisons ($p < 0.05$). For the difference spectrogram, the black contour lines indicate statistical significance of permutation of condition labels, after FDR correction for multiple comparisons ($p < 0.05$). The far right panel shows average z scores from 0-4 seconds post sniff for each frequency band for odor and no-odor trials. **B-C**. Results from individual analysis showing Z-normalized amplitude spectrograms for odor (B) and no-odor (C) conditions for each participant, with the average respiratory signal shown on each panel (overlaid red line). Dashed lines represent inhale onset. Black contour lines indicate statistical significance of permutation tests against pre-cue baseline, after FDR correction for multiple comparisons ($p < 0.05$). **D**. Individual theta, beta and gamma summed magnitudes over 0-2s post sniff. Each dot represents data from a single participant, and lines connect data within the same participant. Asterisk indicates statistical significance (paired t test across odor and no-odor conditions ($p < 0.05$)).

Figure 3: Odor-evoked theta, beta and gamma oscillations have different time courses relative to sniff onset. **A**. Percent-amplitude-change time series for odor (blue line) and no-odor (red line) conditions for each frequency band. Shaded areas indicate one standard deviation from the mean across all trials. Thick black lines above indicate statistically significant differences between conditions (FDR corrected $p < 0.05$, paired t test). **B**. Bootstrap colormap of z-normalized amplitude for each frequency band, with results from each repetition stacked along the Y axis. Vertical stripes of consistent color indicate consistent amplitudes across subsampled sets of trials. **C**. Colored shaded areas represent clusters of statistical significance of the trial-by-trial baseline-corrected amplitude time series, for each frequency band (cluster correction test $p < 0.05$, corrected). Upper boundaries of the shaded areas represent the t statistic from the one-sample t test of baseline-corrected amplitude at each time point against 0. Scales for t statistics are shown to the left of each cluster. Overlaid darker dots indicate the average timing of the bootstrapped distribution of peak amplitude occurrence for each frequency band, for each participant. Each dot represents data from one participant. Dots from the same participant are connected by black lines. On the right, cluster masses in relation to the permuted null distribution for each frequency band are shown, with actual values represented by the vertical red line. **D**. Respiratory phase angle distributions corresponding to bootstrapped peak amplitudes for each frequency band. Scale of the polar histogram represents pdf of the distribution. Darker lines overlaid on the distribution indicate the mean vector of the phase distribution. Angle and radius represent averaged phase angle and PLV value respectively.

Figure 4: Beta and gamma oscillations predict odor identification accuracy. **A**. Z-normalized spectrograms for correct (left) and incorrect (right) trials separately. Averaged respiratory signals

are overlayed on each spectrogram (red lines). Dashed lines represent sniff onset. Black contours indicate statistical significance of permutation test against pre-cue baseline, after FDR correction for multiple comparisons ($p < 0.05$). **B**. Distribution of z score amplitudes within each frequency band, shown for correct and incorrect trials separately (upper left and right and lower left panels). The lower right panel shows box plots for the bootstrapped distributions of the difference between correct and incorrect trials. Boxes represent the 25th to 75th percentile of each distribution, the central marker indicates median, and whiskers extend to the extremes of the data excluding outliers. Colored dots represent raw difference values for each distribution. **C**. Bar plots of bootstrapped Pearson's correlation coefficients computed between odor-induced oscillatory amplitudes and task accuracy for each frequency band, over the inhale and exhale time periods separately. Error bars indicate 95% confidence interval of the mean. Dashed line indicates FDR threshold for significant r value. Dots represent single correlation coefficient calculated from each bootstrap. **D**. Scatter plots show bootstrapped percent change relative to baseline for correct and incorrect trials, during inhale and exhale time periods for each frequency band. Each dot is the average result from one bootstrap repetition. **E**. Receiver operating characteristic (ROC) curves of linear binary SVM classifier applied to each of the scatter plots in panel C. Black dots represent optimized classifier, area under the curve (AUC) is indicated for each ROC curve.

Figure 5: High frequency odor-induced oscillations are not driven by attention. **A**. Schematic illustration of attended and unattended conditions. Attended no-odor trials were defined as breaths taken during experimental trials, between the cue and the odor. No odor was present, but the participant was in an attended state. Blue area indicates the time of experimental trials, and

pink areas indicates the time between trials. Black boxes indicate the analysis time windows for the different conditions. **B**. Z-normalized spectrograms of attended odor and attended no-odor trials, and the difference between the two. Average respiratory signals are overlayed for each condition (red lines). Dashed line represents inhalation onset. Black contours indicate statistical significance (permutation tests as described elsewhere, FDR corrected $p < 0.05$).

Figure 6: Theta phase modulates higher frequency amplitudes during inhale, when odor is present. **A**. Average magnitude time series of the difference between attended odor and attended no-odor conditions, showing evident beta modulations occurring at theta rhythms (grey box). **B**. Z-normalized modulation index (MI) of theta phase and higher frequency amplitudes (13 to 150 Hz), during 0-1s post sniff for all trials in the odor and no-odor conditions. Dashed line indicates FDR threshold for significant MI (FDR corrected $p < 0.05$).

Methods

Ethics statement

This study was approved by the Institutional Review Board at Northwestern University, and the study adhered to the Declaration of Helsinki and the Belmont Report. Written informed consent was obtained from all participants.

Participants

Our study included iEEG data from seven patients with medication-resistant epilepsy. All participants had depth electrodes implanted stereotactically for clinical pre-surgical evaluation (**Fig. 1A**). Electrode locations were determined solely based on clinical need and, in our

participant population, included piriform cortex within the medial temporal lobe. Data were acquired at Northwestern Memorial Hospital.

Behavioral task

Participants performed a cued odor identification task in which they were asked whether an odor matched a prior cue. This task involved periodic presentation of cued odors with time periods between odor trials exceeding 6x the respiratory period of each individual. During this intertrial period, participants breathed naturally through the nose, and no odor was presented. The experimental trials were conducted in each participant's the hospital room, and were computer-controlled, presented to participants using an Apple laptop computer running MATLAB (RRID: SCR_001622) via the *PsychToolBox* extension (RRID: SCR_ 002881). Each trial of the task began with an auditory cue consisting of either the word "rose" or "mint". The cue was delivered by computer speaker using a laptop placed in front of the patients. After a delay of 3 to 7 seconds, the odor of rose (essential oil) or mint (methyl salicylate) was delivered through opaque squeeze bottles, while nasal airflow was monitored in order to precisely determine sniff onsets. The participant was then prompted to indicate their response via button press. The timing of experimental events were synchronized with the ongoing iEEG data through use of a data acquisition board (USB-1208F, Measurement Computing), which translated TTL pulses from MATLAB into the clinical EEG acquisition system (Nihon Kohden, Japan).

iEEG and respiratory signal recording

iEEG signals were recorded using the clinical EEG data acquisition system (Nihon Kohden, Tokyo Japan) that is currently in use in Northwestern Memorial Hospital. The sampling rate for each participant was determined clinically, and ranged from 500Hz to 2000Hz across participants. The reference and ground consisted of an implanted electrode strip on the surface of the brain facing the scalp. We recorded nasal airflow using a piezoelectric pressure sensor (Salter Labs Model #5500) with a nasal cannula placed at the patients' nostrils during the experiment. Nasal airflow signals were recorded directly into the clinical acquisition system, and were therefore automatically synchronized with the iEEG data. The signal was first mean centered, then key respiratory features—including inhale and exhale onset, respiratory peak, and trough volume and time—were detected automatically with MATLAB toolbox *breathmetrics* developed by our lab (Noto et al., 2018), and then manually confirmed.

Electrode Localization

As previously described (Arabkheradmand et al., 2020; Zhou et al., 2019), to determine the implanted electrode locations, the post-operative computed tomography (CT) images were registered to individual pre-operative structural MRI images using FSL's linear registration tool. The transformed post-operative CT images were thresholded, and each electrode was identified manually. We used the center of each identified electrode as its coordinate in individual anatomical space. A single piriform cortex contact was identified on each individual brain image based on the human brain atlas (Mai et al., 2015).

Time-frequency analysis

For all time-frequency analyses, filtering was conducted using a two-pass, zero-phase-lag, finite impulse response (FIR) filter, as implemented by the MATLAB toolbox *fieldtrip* (RRID: SCR_004849), unless specified otherwise. We first low-pass filtered the iEEG signal at 235Hz and then removed 60Hz noise and its harmonics with a band-stop filter with a bandwidth of 4Hz. We then downsampled the signal to 500Hz and re-referenced the data to the common average. To compute spectrograms, we filtered the pre-processed data between 1 to 200 Hz in 100 logarithmically increasing steps ranging from 2 to 50Hz in width. We kept only the first 95 frequency bands from 1 to 153 Hz as our frequencies of interest for all subsequent analyses unless specified otherwise. The analytical amplitudes of the filtered signals were calculated by taking the absolute value of the Hilbert-transformed signal, and temporally smoothed with a moving average filter kernel of 10ms.

To compute spectrograms, we first created sniff-onset-aligned epochs, extending from -2s prior to 4s following the sniff onset, for each trial. Sniff onsets were determined using *breathmetrics* (Noto et al., 2018). Sniffs taken during experimental trials at the time of odor presentation were used for the odor condition, sniffs taken in between trials when no odor was present were used for the no-odor condition, and sniffs taken during experimental trials in between the cue and odor were used for the attended-no-odor condition. There were a larger number of no-odor trials compared to odor trials, and therefore, no-odor trials were randomly sampled without replacement for each participant separately to match trial numbers across conditions for further analysis. The spectrograms were calculated by averaging the amplitude epochs across trials at each frequency, which was further normalized by subtracting the baseline relative to cue onset. To determine statistical significance, we used a permutation method (Arabkheradmand et al., 2020; Canolty et al., 2007; Zhou et al., 2019) to generate z score values. For each repetition of

the permutation process, we randomly sampled a point around sniff onset for all trials and calculated the mean across trials. This process was repeated 10,000 times to create a null distribution of amplitude values around sniff onset. We computed the null distributions for the combined analysis and for each participant separately, and normalized the trial-wise averaged amplitude to the corresponding null distributions. For difference spectrograms, we took the mean of each time/frequency point within each condition and calculated the difference across conditions. To compute statistical significance, we used an exchange-label permutation method, in which we pooled all odor and no-odor trials, randomly assigned a label to each trial, and calculated a cross-conditional difference for each repetition. This process was repeated 10,000 times to create a null distribution of difference values for every time/frequency point, which was used to z-normalize the real difference matrix. The spectrograms created for the attentional control analysis shown in Figure 4B were generated with the same methods, with the number of trials adjusted to include equal numbers of odor and attended-no-odor trials.

To compute the percent amplitude change time series shown in Fig 3A, we first calculated the amplitude for each frequency band separately (theta 4-8Hz, beta 13-30Hz, gamma 30-150Hz), at each time point, by averaging the amplitudes extracted from all sub-bands. To directly compare amplitudes at each time point for odor vs. no odor conditions, we calculated the percent change relative to baseline (-500ms to -50ms relative to cue onset) for each trial [(Amp-Amp_bsl)/Amp_bsl]. In this way, we created a trial by time-percent-change matrix for each frequency band and for each condition, (odor vs. no odor) respectively. We then performed paired sample t tests at each time point across odor vs. no odor trials to test for statistical significance at each time point. FDR correction was used to correct for multiple comparisons.

In order to visualize the differences in temporal dynamics across frequency bands, we used a bootstrapping method to create z-normalized amplitude colormaps for each frequency band (**Fig 3B**). To do this, we first baseline corrected and z-normalized all trials. For each repetition, we resampled all 323 trials with replacement, averaged across trials, and averaged across sub-bands for each frequency band in order to create a single z-score time series for each frequency band. This process was repeated 2000 times to generate a repetition (Y axis of Fig 3B) by time, z-score matrix for each frequency band.

We then performed a cluster-based analysis to quantify the time course of significant responses for each frequency band (**Fig. 3C**). To do this, for each frequency band, we first performed one sample t tests against zero for z-normalized amplitudes for all trials at each time point, creating a time series of t-statistics. We then performed a cluster-based statistical thresholding analysis (Maris & Oostenveld, 2007) in order to identify continuous, significant clusters within the t-statistic time series for each frequency band. The cluster mass was defined as the sum of the t-statistics of a given cluster (Maris & Oostenveld, 2007). Subsequently, permutation-based correction for multiple comparisons was conducted in order to eliminate all small clusters that were likely to be caused by chance. Specifically, for each repetition, we circularly shifted a random number of trials, recalculated the t-statistics, applied the same threshold, and then saved the cluster mass of the maximal cluster. This process was repeated 10,000 times to create a null distribution of cluster masses. We took the 95th percentile of this distribution as the cutoff and kept all clusters that were larger than this threshold.

We next conducted an analysis to explore the timing and phase of responses in each frequency band (**Fig. 3D**). We used a bootstrap method to calculate the distribution of respiratory phase

values at which the peak amplitude responses occurred for each frequency. We resampled all 323 trials (with replacement), keeping both the LFP and breathing signals. For each repetition, we used the Hilbert transform to extract respiratory phase values. We used a sliding window of 50ms to extract the maximal LFP amplitude responses by calculating and comparing mean amplitudes within each window across the entire 4s post-sniff time period. Phase angles corresponding to the center of the window in which the maximal amplitude occurred were used, and plotted on a polar histogram. We then computed the PLV (Aydore et al., 2013) and average phase angle of these phase distributions using the MATLAB toolbox *circstats* (Berens, 2009) (RRID: SCR_016651). The Rayleigh test was performed to test for the non-uniformity of phase distributions. For the peak timing analysis on the single participant level, we used the same method.

We next conducted a series of analyses to look for relationships between LFPs and odor identification accuracy (**Fig 4**). First, to statistically compare the amplitude difference between correct and incorrect trials, we conducted a resampling analysis. For each repetition, we resampled equal numbers of correct and incorrect trials (71, with replacement) to ensure a fair comparison across conditions. On each repetition, we calculated the mean of z-normalized amplitudes across the entire time window for each frequency band, subtracted the mean of incorrect trials from the mean of correct trials, and repeated this process 200 times to generate the distribution of difference values between correct and incorrect trials. The difference distribution for each frequency band was tested against 0 using one-sample t tests to generate statistics. The distribution was plotted as scatter as well as box plot.

To look for relationships between LFP amplitudes and task accuracy (**Fig. 4C**), for each repetition (1000x) in a bootstrapped-correlation analysis, we resampled (with replacement) and averaged all trials. We then calculated the mean amplitude during inhale and exhale separately (inhale-exhale transition defined by phase angle of pi/2 for averaged breathing signal) for all three frequency bands. We calculated Pearson's correlation coefficients between task accuracy and mean amplitudes for inhale and exhale, for each frequency band. We then repeated this entire process 50 times. We used FDR to correct for multiple comparisons ($p<0.05$). We subsequently fisher-z-transformed all Pearson's r values and conducted a repeated measures two-way ANOVA as well as paired sample t tests to analyze the differences across frequency bands and respiratory phases.

We next created scatter plot visualizations of responses across inhale and exhale phases **(Fig. 4D-E).** To balance the discrepancy between correct and incorrect trial numbers (252 vs. 71), we conducted a bootstrapping analysis using equal numbers of trials across conditions on each repetition. We first computed the mean amplitudes during inhale and exhale for each frequency band. For each respiratory phase and frequency band, we sampled 30 trials with replacement each time, calculated percent change relative to baseline with the trial-wise averaged amplitude time series, and calculated average amplitudes during inhale and exhale for each trial set. Inhale and exhale periods were defined as 0-1.5s and 1.5-3s post sniff respectively for all trials. This process was repeated 500 times for both correct and incorrect trials to generate a scatterplot of corresponding inhale and exhale amplitudes for trials from both conditions. In order to test the separability of data, we applied a linear binary SVM classifier using MATLAB function *fitcsvm* with five-fold cross validation. ROC curves were generated using the function *perfcurve.*

phase-amplitude coupling analysis

We calculated the modulation index (MI) to measure coupling between theta phase and higher frequency amplitudes (13-150Hz) (**Fig. 5**). To do so, we extracted the phase angle time series for the theta frequency band (4-8Hz), and then from that phase time series, created sniff-aligned trial epochs. Data from all trials was concatenated. To generate the higher frequency amplitude data that was used to compute the MI, the raw time series were filtered and amplitude-extracted (as described previously) to the same 47 log-spaced frequency bands (13.05- 153.04 Hz), with logarithmically increasing bandwidth, as described in the previous section for the time-frequency analysis. We then concatenated this data identically to the theta phase data. MI was calculated as the Kullbach-Leibner distance divided by the logged number of bins (Tort et al., 2010). To normalize the MI, we created a null distribution of MI values. For each repetition, and for each frequency band, we circularly shifted the concatenated amplitude time series, and calculated the MI between the shifted amplitudes and theta phase values. This process was repeated 1000 times for each frequency band to generate the corresponding null distribution of MI values. We then normalized the raw MI to the null distributions to generate the z-scores, and FDR corrected for multiple comparisons.

REFERENCES:

Adrian, E. D. (1942). Olfactory reactions in the brain of the hedgehog. *The Journal of Physiology*, *100*(4), 459-473. https://doi.org/10.1113/jphysiol.1942.sp003955 PMID - 16991539

Arabkheradmand, G., Zhou, G., Noto, T., Yang, Q., Schuele, S. U., Parvizi, J., Gottfried, J. A., Wu, S., Rosenow, J. M., Koubeissi, M. Z., Lane, G., & Zelano, C. (2020). Anticipation-induced delta phase reset improves human olfactory perception. *PLOS Biology*, *18*(5), e3000724. https://doi.org/10.1371/journal.pbio.3000724 PMID - 32453719

Arshamian, A., Iravani, B., Majid, A., & Lundström, J. N. (2018). Respiration modulates olfactory memory consolidation in humans. *Journal of Neuroscience*, *38*(48), 3360-3317. https://doi.org/10.1523/jneurosci.3360-17.2018 PMID - 30348674

Arzi, A., Rozenkrantz, L., Holtzman, Y., Secundo, L., & Sobel, N. (2014). Sniffing patterns uncover implicit memory for undetected odors. *Current Biology*, *24*(7), R263-R264. https://doi.org/10.1016/j.cub.2014.02.004 PMID - 24698370

Arzi, A., Sela, L., Green, A., Givaty, G., Dagan, Y., & Sobel, N. (2010). The Influence of Odorants on Respiratory Patterns in Sleep. *Chemical Senses*, *35*(1), 31-40. https://doi.org/10.1093/chemse/bjp079 PMID - 19917590

Aydore, S., Pantazis, D., & Leahy, R. M. (2013). A note on the phase locking value and its properties. *NeuroImage*, *74*, 231-244. https://doi.org/10.1016/j.neuroimage.2013.02.008 PMID - 23435210

Başar, E., Başar-Eroglu, C., Karakaş, S., & Schürmann, M. (2001). Gamma, alpha, delta, and theta oscillations govern cognitive processes. *International Journal of Psychophysiology*, *39*(2-3), 241-248. https://doi.org/10.1016/s0167-8760(00)00145-8 PMID - 11163901

Bathellier, B., Buhl, D. L., Accolla, R., & Carleton, A. (2008). Dynamic Ensemble Odor Coding in the Mammalian Olfactory Bulb: Sensory Information at Different Timescales. *Neuron*, *57*(4), 586-598. https://doi.org/10.1016/j.neuron.2008.02.011 PMID - 18304487

Berens, P. (2009). CircStat: a MATLAB toolbox for circular statistics. *J Stat Softw*, *31*(10), 1-21.

Beshel, J., Kopell, N., & Kay, L. M. (2007). Olfactory Bulb Gamma Oscillations Are Enhanced with Task Demands. *The Journal of Neuroscience*, *27*(31), 8358-8365. https://doi.org/10.1523/jneurosci.1199-07.2007 PMID - 17670982

Bhutani, S., Howard, J. D., Reynolds, R., Zee, P. C., Gottfried, J., & Kahnt, T. (2019). Olfactory connectivity mediates sleep-dependent food choices in humans. *eLife*, *8*, e49053. https://doi.org/10.7554/elife.49053 PMID - 31591965

Blauvelt, D. G., Sato, T. F., Wienisch, M., Knöpfel, T., & Murthy, V. N. (2013). Distinct spatiotemporal activity in principal neurons of the mouse olfactory bulb in anesthetized and awake states. *Frontiers in Neural Circuits*, *7*, 46. https://doi.org/10.3389/fncir.2013.00046 PMID - 23543674

Bolding, K. A., & Franks, K. M. (2017). Complementary codes for odor identity and intensity in olfactory cortex. *eLife*, *6*, e22630. https://doi.org/10.7554/elife.22630 PMID - 28379135

Buonviso, N., Amat, C., Litaudon, P., Roux, S., Royet, J. P., Farget, V., & Sicard, G. (2003). Rhythm sequence through the olfactory bulb layers during the time window of a respiratory cycle. *European Journal of Neuroscience*, *17*(9), 1811-1819. https://doi.org/10.1046/j.1460-9568.2003.02619.x PMID - 12752780

Buzsáki, G. (2002). Theta Oscillations in the Hippocampus. *Neuron*, *33*(3), 325-340. https://doi.org/10.1016/s0896-6273(02)00586-x PMID - 11832222

Buzsáki, G., & Wang, X.-J. (2012). Mechanisms of Gamma Oscillations. *Annual Review of Neuroscience*, *35*(1), 203-225. https://doi.org/10.1146/annurev-neuro-062111-150444 PMID - 22443509

Canolty, R. T., Soltani, M., Dalal, S. S., Edwards, E., Dronkers, N. F., Nagarajan, S. S., Kirsch, H. E., Barbaro, N. M., & Knight, R. T. (2007). Spatiotemporal dynamics of word processing in the human brain. *Frontiers in neuroscience*, *1*(1), 185-196. https://doi.org/10.3389/neuro.01.1.1.014.2007 PMID - 18982128

Carlson, K. S., Gadziola, M. A., Dauster, E. S., & Wesson, D. W. (2018). Selective Attention Controls Olfactory Decisions and the Neural Encoding of Odors. *Current Biology*, *28*(14), 2195-2205.e2194. https://doi.org/10.1016/j.cub.2018.05.011 PMID - 30056854

Cenier, T., Amat, C., Litaudon, P., Garcia, S., Micheaux, P. L. d., Liquet, B., Roux, S., & Buonviso, N. (2008). Odor vapor pressure and quality modulate local field potential oscillatory patterns in the olfactory bulb of the anesthetized rat. *European Journal of Neuroscience*, *27*(6), 1432-1440. https://doi.org/10.1111/j.1460-9568.2008.06123.x PMID - 18364022

Chapuis, J., Cohen, Y., He, X., Zhang, Z., Jin, S., Xu, F., & Wilson, D. A. (2013). Lateral Entorhinal Modulation of Piriform Cortical Activity and Fine Odor Discrimination. *The Journal of Neuroscience*, *33*(33), 13449-13459. https://doi.org/10.1523/jneurosci.1387-13.2013 PMID - 23946403

Cohen, Y., Putrino, D., & Wilson, D. A. (2015). Dynamic cortical lateralization during olfactory discrimination learning. *The Journal of Physiology*, *593*(7), 1701-1714. https://doi.org/10.1113/jphysiol.2014.288381 PMID - 25604039

Courtiol, E., Buonviso, N., & Litaudon, P. (2019). Odorant Features Differentially Modulate Beta/Gamma Oscillatory Patterns in Anterior Versus Posterior Piriform Cortex. *Neuroscience*, *409*, 26-34. https://doi.org/10.1016/j.neuroscience.2019.04.025 PMID - 31022464

David, F., Courtiol, E., Buonviso, N., & Fourcaud-Trocmé, N. (2015). Competing Mechanisms of Gamma and Beta Oscillations in the Olfactory Bulb Based on Multimodal Inhibition of Mitral Cells Over a Respiratory Cycle. *eNeuro*, *2*(6), ENEURO.0018-0015.2015. https://doi.org/10.1523/eneuro.0018-15.2015 PMID - 26665163

Engel, A. K., & Fries, P. (2010). Beta-band oscillations—signalling the status quo? *Current Opinion in Neurobiology*, *20*(2), 156-165. https://doi.org/10.1016/j.conb.2010.02.015 PMID - 20359884

Fontanini, A., & Bower, J. M. (2006). Slow-waves in the olfactory system: an olfactory perspective on cortical rhythms. *Trends in Neurosciences*, *29*(8), 429-437. https://doi.org/10.1016/j.tins.2006.06.013 PMID - 16842864

Frederick, D. E., Brown, A., Brim, E., Mehta, N., Vujovic, M., & Kay, L. M. (2016). Gamma and Beta Oscillations Define a Sequence of Neurocognitive Modes Present in Odor Processing. *The Journal of neuroscience : the official journal of the Society for Neuroscience*, *36*(29), 7750-7767. https://doi.org/10.1523/jneurosci.0569-16.2016 PMID - 27445151

Frederick, D. E., Brown, A., Tacopina, S., Mehta, N., Vujovic, M., Brim, E., Amina, T., Fixsen, B., & Kay, L. M. (2017). Task-Dependent Behavioral Dynamics Make the Case for Temporal Integration in Multiple Strategies during Odor Processing. *The Journal of Neuroscience*, *37*(16), 4416-4426. https://doi.org/10.1523/jneurosci.1797-16.2017 PMID - 28336570

Fröhlich, F., & McCormick, D. A. (2010). Endogenous Electric Fields May Guide Neocortical Network Activity. *Neuron*, *67*(1), 129-143. https://doi.org/10.1016/j.neuron.2010.06.005 PMID - 20624597

Fukunaga, I., Herb, J. T., Kollo, M., Boyden, E. S., & Schaefer, A. T. (2014). Independent control of gamma and theta activity by distinct interneuron networks in the olfactory bulb. *Nature Neuroscience*, *17*(9), 1208-1216. https://doi.org/10.1038/nn.3760 PMID - 24997762

Gnaedinger, A., Gurden, H., Gourévitch, B., & Martin, C. (2019). Multisensory learning between odor and sound enhances beta oscillations. *Scientific Reports*, *9*(1), 11236. https://doi.org/10.1038/s41598-019-47503-y PMID - 31375760

Grosmaitre, X., Santarelli, L. C., Tan, J., Luo, M., & Ma, M. (2007). Dual functions of mammalian olfactory sensory neurons as odor detectors and mechanical sensors. *Nature Neuroscience*, *10*(3), 348-354. https://doi.org/10.1038/nn1856 PMID - 17310245

Haddad, R., Lanjuin, A., Madisen, L., Zeng, H., Murthy, V. N., & Uchida, N. (2013). Olfactory cortical neurons read out a relative time code in the olfactory bulb. *Nature Neuroscience*, *16*(7), 949-957. https://doi.org/10.1038/nn.3407 PMID - 23685720

Hauner, K. K., Howard, J. D., Zelano, C., & Gottfried, J. A. (2013). Stimulus-specific enhancement of fear extinction during slow-wave sleep. *Nature Neuroscience*, *16*(11), 1553-1555. https://doi.org/10.1038/nn.3527 PMID - 24056700

Heck, D. H., McAfee, S. S., Liu, Y., Babajani-Feremi, A., Rezaie, R., Freeman, W. J., Wheless, J. W., Papanicolaou, A. C., Ruszinkó, M., Sokolov, Y., & Kozma, R. (2017). Breathing as a Fundamental Rhythm of Brain Function. *Frontiers in Neural Circuits*, *10*, 115. https://doi.org/10.3389/fncir.2016.00115 PMID - 28127277

Herrero, J. L., Khuvis, S., Yeagle, E., Cerf, M., & Mehta, A. D. (2018). Breathing above the brain stem: volitional control and attentional modulation in humans. *Journal of Neurophysiology*, *119*(1), 145-159. https://doi.org/10.1152/jn.00551.2017 PMID - 28954895

Howard, J. D., Reynolds, R., Smith, D. E., Voss, J. L., Schoenbaum, G., & Kahnt, T. (2020). Targeted Stimulation of Human Orbitofrontal Networks Disrupts Outcome-Guided Behavior. *Current Biology*, *30*(3), 490-498.e494. https://doi.org/10.1016/j.cub.2019.12.007 PMID - 31956033

Hudry, J., Ryvlin, P., Royet, J.-P., & Mauguière, F. (2001). Odorants Elicit Evoked Potentials in the Human Amygdala. *Cerebral Cortex*, *11*(7), 619-627. https://doi.org/10.1093/cercor/11.7.619 PMID - 11415964

Iravani, B., Arshamian, A., Ohla, K., Wilson, D. A., & Lundström, J. N. (2020). Non-invasive recording from the human olfactory bulb. *Nature Communications*, *11*(1), 648. https://doi.org/10.1038/s41467-020-14520-9 PMID - 32005822

Iurilli, G., & Datta, S. R. (2017). Population Coding in an Innately Relevant Olfactory Area. *Neuron*, *93*(5), 1180-1197.e1187. https://doi.org/10.1016/j.neuron.2017.02.010 PMID - 28238549

Jessberger, J., Zhong, W., Brankačk, J., & Draguhn, A. (2016). Olfactory Bulb Field Potentials and Respiration in Sleep-Wake States of Mice. *Neural Plasticity*, *2016*, 1-9. https://doi.org/10.1155/2016/4570831 PMID - 27247803

Jiang, H., Schuele, S., Rosenow, J., Zelano, C., Parvizi, J., Tao, J. X., Wu, S., & Gottfried, J. A. (2017). Theta Oscillations Rapidly Convey Odor-Specific Content in Human Piriform Cortex. *Neuron*, *94*(1), 207-219.e204. https://doi.org/10.1016/j.neuron.2017.03.021 PMID - 28384472

Jung, J., Hudry, J., Ryvlin, P., Royet, J.-P., Bertrand, O., & Lachaux, J.-P. (2006). Functional Significance of Olfactory-induced Oscillations in the Human Amygdala. *Cerebral Cortex*, *16*(1), 1-8. https://doi.org/10.1093/cercor/bhi090 PMID - 15829732

Kam, J. W. Y., Lin, J. J., Solbakk, A.-K., Endestad, T., Larsson, P. G., & Knight, R. T. (2019). Default network and frontoparietal control network theta connectivity supports internal attention. *Nature Human Behaviour*, *3*(12), 1263-1270. https://doi.org/10.1038/s41562-019-0717-0 PMID - 31477910

Kay, L. M. (2005). Theta oscillations and sensorimotor performance. *Proceedings of the National Academy of Sciences*, *102*(10), 3863-3868. https://doi.org/10.1073/pnas.0407920102 PMID - 15738424

Kay, L. M. (2014). Progress in Brain Research. *Progress in Brain Research*, *208*, 223-251. https://doi.org/10.1016/b978-0-444-63350-7.00009-7 PMID - 24767485

Kay, L. M., & Beshel, J. (2010). A Beta Oscillation Network in the Rat Olfactory System During a 2-Alternative Choice Odor Discrimination Task. *Journal of Neurophysiology*, *104*(2), 829-839. https://doi.org/10.1152/jn.00166.2010 PMID - 20538778

Kay, L. M., Beshel, J., Brea, J., Martin, C., Rojas-Líbano, D., & Kopell, N. (2009). Olfactory oscillations: the what, how and what for. *Trends in Neurosciences*, *32*(4), 207-214. https://doi.org/10.1016/j.tins.2008.11.008 PMID - 19243843

Kay, L. M., & Stopfer, M. (2006). Information processing in the olfactory systems of insects and vertebrates. *Seminars in Cell & Developmental Biology*, *17*(4), 433-442. https://doi.org/10.1016/j.semcdb.2006.04.012 PMID - 16766212

Kepecs, A., Uchida, N., & Mainen, Z. F. (2006). The Sniff as a Unit of Olfactory Processing. *Chemical Senses*, *31*(2), 167-179. https://doi.org/10.1093/chemse/bjj016 PMID - 16339265

Kepecs, A., Uchida, N., & Mainen, Z. F. (2007). Rapid and Precise Control of Sniffing During Olfactory Discrimination in Rats. *Journal of Neurophysiology*, *98*(1), 205-213. https://doi.org/10.1152/jn.00071.2007 PMID - 17460109

Ketchum, K. L., & Haberly, L. B. (1993). Synaptic events that generate fast oscillations in piriform cortex. *The Journal of Neuroscience*, *13*(9), 3980-3985. https://doi.org/10.1523/jneurosci.13-09-03980.1993 PMID - 8366356

Kopell, N., Ermentrout, G. B., Whittington, M. A., & Traub, R. D. (2000). Gamma rhythms and beta rhythms have different synchronization properties. *Proceedings of the National Academy of Sciences*, *97*(4), 1867-1872. https://doi.org/10.1073/pnas.97.4.1867 PMID - 10677548

Lepousez, G., & Lledo, P.-M. (2013). Odor Discrimination Requires Proper Olfactory Fast Oscillations in Awake Mice. *Neuron*, *80*(4), 1010-1024. https://doi.org/10.1016/j.neuron.2013.07.025 PMID - 24139818

Lisman, John E., & Jensen, O. (2013). The Theta-Gamma Neural Code. *Neuron*, *77*(6), 1002-1016. https://doi.org/10.1016/j.neuron.2013.03.007 PMID - 23522038

Litaudon, P., Garcia, S., & Buonviso, N. (2008). Strong coupling between pyramidal cell activity and network oscillations in the olfactory cortex. *Neuroscience*, *156*(3), 781-787. https://doi.org/10.1016/j.neuroscience.2008.07.077 PMID - 18790020

Lockmann, A. L. V., Laplagne, D. A., & Tort, A. B. L. (2018). Olfactory bulb drives respiration-coupled beta oscillations in the rat hippocampus. *European Journal of Neuroscience*, *48*(8), 2663-2673. https://doi.org/10.1111/ejn.13665 PMID - 28833629

Losacco, J., Ramirez-Gordillo, D., Gilmer, J., & Restrepo, D. (2020). Learning improves decoding of odor identity with phase-referenced oscillations in the olfactory bulb. *eLife*, *9*, e52583. https://doi.org/10.7554/elife.52583 PMID - 31990271

Lowry, C. A., & Kay, L. M. (2007). Chemical Factors Determine Olfactory System Beta Oscillations in Waking Rats. *Journal of Neurophysiology*, *98*(1), 394-404. https://doi.org/10.1152/jn.00124.2007 PMID - 17442770

Macrides, F., Eichenbaum, H. B., & Forbes, W. B. (1982). Temporal relationship between sniffing and the limbic theta rhythm during odor discrimination reversal learning. *Journal of Neuroscience*, *2*(12), 1705-1717. https://doi.org/10.1523/jneurosci.02-12-01705.1982 PMID - 7143047

Mai, J. K., Majtanik, M., & Paxinos, G. (2015). *Atlas of the human brain*. Academic Press.

Mainland, J., & Sobel, N. (2006). The sniff is part of the olfactory percept. *Chemical Senses*, *31*(2), 181-196.

Majid, A. (2020). Human Olfaction at the Intersection of Language, Culture, and Biology. *Trends in Cognitive Sciences*, *25*(2), 111-123. https://doi.org/10.1016/j.tics.2020.11.005 PMID - 33349546

Majid, A., & Kruspe, N. (2018). Hunter-Gatherer Olfaction Is Special. *Current Biology*, *28*(3), 409-413.e402. https://doi.org/10.1016/j.cub.2017.12.014 PMID - 29358070

Manabe, H., & Mori, K. (2013). Sniff rhythm-paced fast and slow gamma-oscillations in the olfactory bulb: relation to tufted and mitral cells and behavioral states. *Journal of Neurophysiology*, *110*(7), 1593-1599. https://doi.org/10.1152/jn.00379.2013 PMID - 23864376

Maris, E., & Oostenveld, R. (2007). Nonparametric statistical testing of EEG- and MEG-data. *Journal of Neuroscience Methods*, *164*(1), 177-190. https://doi.org/10.1016/j.jneumeth.2007.03.024 PMID - 17517438

Martin, C., Beshel, J., & Kay, L. M. (2007). An Olfacto-Hippocampal Network Is Dynamically Involved in Odor-Discrimination Learning. *Journal of Neurophysiology*, *98*(4), 2196-2205. https://doi.org/10.1152/jn.00524.2007 PMID - 17699692

Martin, C., & Ravel, N. (2014). Beta and gamma oscillatory activities associated with olfactory memory tasks: different rhythms for different functional networks? *Frontiers in Behavioral Neuroscience*, *8*, 218. https://doi.org/10.3389/fnbeh.2014.00218 PMID - 25002840

Millman, D. J., & Murthy, V. N. (2020). Rapid Learning of Odor–Value Association in the Olfactory Striatum. *The Journal of Neuroscience*, *40*(22), 4335-4347. https://doi.org/10.1523/jneurosci.2604-19.2020 PMID - 32321744

Moberly, A. H., Schreck, M., Bhattarai, J. P., Zweifel, L. S., Luo, W., & Ma, M. (2018). Olfactory inputs modulate respiration-related rhythmic activity in the prefrontal cortex and

freezing behavior. *Nature Communications*, *9*(1), 1528. https://doi.org/10.1038/s41467-018-03988-1 PMID - 29670106

Mori, K., Manabe, H., Narikiyo, K., & Onisawa, N. (2013). Olfactory consciousness and gamma oscillation couplings across the olfactory bulb, olfactory cortex, and orbitofrontal cortex. *Frontiers in Psychology*, *4*, 743. https://doi.org/10.3389/fpsyg.2013.00743 PMID - 24137148

Neville, K. R., & Haberly, L. B. (2003). Beta and Gamma Oscillations in the Olfactory System of the Urethane-Anesthetized Rat. *Journal of Neurophysiology*, *90*(6), 3921-3930. https://doi.org/10.1152/jn.00475.2003 PMID - 12917385

Noto, T., Zhou, G., Schuele, S., Templer, J., & Zelano, C. (2018). Automated analysis of breathing waveforms using BreathMetrics: a respiratory signal processing toolbox. *Chemical Senses*, *43*(8), 583-597. https://doi.org/10.1093/chemse/bjy045 PMID - 29985980

Olofsson, J. K., & Gottfried, J. A. (2015). The muted sense: neurocognitive limitations of olfactory language. *Trends in Cognitive Sciences*, *19*(6), 314-321. https://doi.org/10.1016/j.tics.2015.04.007 PMID - 25979848

Perl, O., Arzi, A., Sela, L., Secundo, L., Holtzman, Y., Samnon, P., Oksenberg, A., Sobel, N., & Hairston, I. S. (2016). Odors enhance slow-wave activity in non-rapid eye movement sleep. *Journal of Neurophysiology*, *115*(5), 2294-2302. https://doi.org/10.1152/jn.01001.2015 PMID - 26888107

Phillips, M. E., Sachdev, R. N. S., Willhite, D. C., & Shepherd, G. M. (2012). Respiration Drives Network Activity and Modulates Synaptic and Circuit Processing of Lateral Inhibition in the Olfactory Bulb. *The Journal of Neuroscience*, *32*(1), 85-98. https://doi.org/10.1523/jneurosci.4278-11.2012 PMID - 22219272

Poo, C., & Isaacson, J. S. (2009). Odor Representations in Olfactory Cortex: "Sparse" Coding, Global Inhibition, and Oscillations. *Neuron*, *62*(6), 850-861. https://doi.org/10.1016/j.neuron.2009.05.022 PMID - 19555653

Rasch, B., Büchel, C., Gais, S., & Born, J. (2007). Odor Cues During Slow-Wave Sleep Prompt Declarative Memory Consolidation. *Science*, *315*(5817), 1426-1429. https://doi.org/10.1126/science.1138581 PMID - 17347444

Ravel, N., Chabaud, P., Martin, C., Gaveau, V., Hugues, E., Tallon‐Baudry, C., Bertrand, O., & Gervais, R. (2003). Olfactory learning modifies the expression of odour‐induced oscillatory responses in the gamma (60–90 Hz) and beta (15–40 Hz) bands in the rat olfactory bulb. *European Journal of Neuroscience*, *17*(2), 350-358. https://doi.org/10.1046/j.1460-9568.2003.02445.x PMID - 12542672

Rennaker, R. L., Chen, C.-F. F., Ruyle, A. M., Sloan, A. M., & Wilson, D. A. (2007). Spatial and Temporal Distribution of Odorant-Evoked Activity in the Piriform Cortex. *The Journal of Neuroscience*, *27*(7), 1534-1542. https://doi.org/10.1523/jneurosci.4072-06.2007 PMID - 17301162

Rojas-Líbano, D., Frederick, D. E., Egaña, J. I., & Kay, L. M. (2014). The olfactory bulb theta rhythm follows all frequencies of diaphragmatic respiration in the freely behaving rat. *Frontiers in Behavioral Neuroscience*, *8*, 214. https://doi.org/10.3389/fnbeh.2014.00214 PMID - 24966821

Rosero, M. A., & Aylwin, M. L. (2011). Sniffing shapes the dynamics of olfactory bulb gamma oscillations in awake behaving rats. *European Journal of Neuroscience*, *34*(5), 787-799. https://doi.org/10.1111/j.1460-9568.2011.07800.x PMID - 21819462

Schroeder, C. E., Wilson, D. A., Radman, T., Scharfman, H., & Lakatos, P. (2010). Dynamics of Active Sensing and perceptual selection. *Current Opinion in Neurobiology*, *20*(2), 172-176. https://doi.org/10.1016/j.conb.2010.02.010 PMID - 20307966

Shusterman, R., Smear, M. C., Koulakov, A. A., & Rinberg, D. (2011). Precise olfactory responses tile the sniff cycle. *Nature Neuroscience*, *14*(8), 1039-1044. https://doi.org/10.1038/nn.2877 PMID - 21765422

Sirotin, Y. B., Costa, M. E., & Laplagne, D. A. (2014). Rodent ultrasonic vocalizations are bound to active sniffing behavior. *Frontiers in Behavioral Neuroscience*, *8*, 399. https://doi.org/10.3389/fnbeh.2014.00399 PMID - 25477796

Sobel, N., Prabhakaran, V., Desmond, J. E., Glover, G. H., Goode, R. L., Sullivan, E. V., & Gabrieli, J. D. E. (1998). Sniffing and smelling: separate subsystems in the human olfactory cortex. *Nature*, *392*(6673), 282-286. https://doi.org/10.1038/32654 PMID - 9521322

Stopfer, M., Bhagavan, S., Smith, B. H., & Laurent, G. (1997). Impaired odour discrimination on desynchronization of odour-encoding neural assemblies. *Nature*, *390*(6655), 70-74. https://doi.org/10.1038/36335 PMID - 9363891

Tort, A. B. L., Komorowski, R., Eichenbaum, H., & Kopell, N. (2010). Measuring Phase-Amplitude Coupling Between Neuronal Oscillations of Different Frequencies. *Journal of Neurophysiology*, *104*(2), 1195-1210. https://doi.org/10.1152/jn.00106.2010 PMID - 20463205

Uchida, N., Kepecs, A., & Mainen, Z. F. (2006). Seeing at a glance, smelling in a whiff: rapid forms of perceptual decision making. *Nature Reviews Neuroscience*, *7*(6), 485-491. https://doi.org/10.1038/nrn1933 PMID - 16715056

Verhagen, J. V., Wesson, D. W., Netoff, T. I., White, J. A., & Wachowiak, M. (2007). Sniffing controls an adaptive filter of sensory input to the olfactory bulb. *Nature Neuroscience*, *10*(5), 631-639. https://doi.org/10.1038/nn1892

Wesson, D. W., Donahou, T. N., Johnson, M. O., & Wachowiak, M. (2008). Sniffing Behavior of Mice during Performance in Odor-Guided Tasks. *Chemical Senses*, *33*(7), 581-596. https://doi.org/10.1093/chemse/bjn029 PMID - 18534995

Wilson, D. A., & Stevenson, R. J. (2003). The fundamental role of memory in olfactory perception. *Trends in Neurosciences*, *26*(5), 243-247. https://doi.org/10.1016/s0166-2236(03)00076-6 PMID - 12744840

Wilson, Donald A., & Sullivan, Regina M. (2011). Cortical Processing of Odor Objects. *Neuron*, *72*(4), 506-519. https://doi.org/10.1016/j.neuron.2011.10.027 PMID - 22099455

Yeshurun, Y., Lapid, H., Dudai, Y., & Sobel, N. (2009). The Privileged Brain Representation of First Olfactory Associations. *Current Biology*, *19*(21), 1869-1874. https://doi.org/10.1016/j.cub.2009.09.066 PMID - 19896380

Zelano, C., Bensafi, M., Porter, J., Mainland, J., Johnson, B., Bremner, E., Telles, C., Khan, R., & Sobel, N. (2005). Attentional modulation in human primary olfactory cortex. *Nature Neuroscience*, *8*(1), 114-120. https://doi.org/10.1038/nn1368 PMID - 15608635

Zelano, C., Jiang, H., Zhou, G., Arora, N., Schuele, S., Rosenow, J., & Gottfried, J. A. (2016). Nasal Respiration Entrains Human Limbic Oscillations and Modulates Cognitive Function. *The*

Journal of Neuroscience, *36*(49), 12448-12467. https://doi.org/10.1523/jneurosci.2586-16.2016 PMID - 27927961

Zhou, G., Lane, G., Noto, T., Arabkheradmand, G., Gottfried, J. A., Schuele, S. U., Rosenow, J. M., Olofsson, J. K., Wilson, D. A., & Zelano, C. (2019). Human olfactory-auditory integration requires phase synchrony between sensory cortices. *Nature Communications*, *10*(1), 1168. https://doi.org/10.1038/s41467-019-09091-3 PMID - 30858379

Zhou, Y., Fang, F.-H., Pan, P., Liu, Z.-R., & Ji, Y.-H. (2017). Visual deprivation induce cross-modal enhancement of olfactory perception. *Biochemical and Biophysical Research Communications*, *486*(3), 833-838. https://doi.org/10.1016/j.bbrc.2017.03.140 PMID - 28359762

Zoefel, B., & VanRullen, R. (2017). Oscillatory Mechanisms of Stimulus Processing and Selection in the Visual and Auditory Systems: State-of-the-Art, Speculations and Suggestions. *Frontiers in neuroscience*, *11*, 296. https://doi.org/10.3389/fnins.2017.00296 PMID - 28603483